

Gauge theory applied to magnetic lattices

Original

Gauge theory applied to magnetic lattices / Di Pietro, A.; Ansalone, P.; Basso, V.; Magni, A.; Durin, G.. - In: EUROPHYSICS LETTERS. - ISSN 0295-5075. - 140:4(2022). [[10.1209/0295-5075/aca0ba](https://doi.org/10.1209/0295-5075/aca0ba)]

Availability:

This version is available at: 11583/2982074 since: 2023-09-13T08:40:27Z

Publisher:

IOP Publishing

Published

DOI:[10.1209/0295-5075/aca0ba](https://doi.org/10.1209/0295-5075/aca0ba)

Terms of use:

This article is made available under terms and conditions as specified in the corresponding bibliographic description in the repository

Publisher copyright

(Article begins on next page)



LETTER • OPEN ACCESS

Gauge theory applied to magnetic lattices

To cite this article: A. Di Pietro *et al* 2022 *EPL* **140** 46003

View the [article online](#) for updates and enhancements.

You may also like

- [Characteristics and controllability of vortices in ferromagnetics, ferroelectrics, and multiferroics](#)
Yue Zheng and W J Chen
- [Micromagnetic simulations using Graphics Processing Units](#)
L Lopez-Diaz, D Aurelio, L Torres et al.
- [Magnetic small-angle neutron scattering of bulk ferromagnets](#)
Andreas Michels

Gauge theory applied to magnetic lattices

A. DI PIETRO^{1,2}, P. ANSALONE¹, V. BASSO¹, A. MAGNI¹  and G. DURIN^{1(a)} 

¹*Istituto Nazionale di Ricerca Metrologica - Strada delle Cacce, 91, 10135 Torino, Italy*

²*Politecnico di Torino - Corso Duca degli Abruzzi, 24, 10129 Torino, Italy*

received 9 September 2022; accepted in final form 7 November 2022
published online 22 November 2022

Abstract – The generalizations of micromagnetic exchange including higher order interactions are normally performed phenomenologically. In this paper we combine graph and gauge field theory to provide a new procedure to perform the continuum limit of the Heisenberg model. Our approach allows to simultaneously account for the symmetries of the crystal, the effect of spin-orbit coupling and their interplay. We obtain a micromagnetic theory accounting for the crystal symmetry constraints at all orders in exchange. The form of the micromagnetic Dzyaloshinskii-Moriya interaction in all 32 point groups is calculated at the first order.

 open access

Copyright © 2022 The author(s)

Published by the EPLA under the terms of the [Creative Commons Attribution 4.0 International License](https://creativecommons.org/licenses/by/4.0/) (CC BY). Further distribution of this work must maintain attribution to the author(s) and the published article's title, journal citation, and DOI.

Introduction. – The Heisenberg model [1–3] is a low energy limit of the more general Hubbard model [4,5] and it allows to translate the complexity of quantum mechanical exchange in a geometrical framework where the degrees of freedom are localized magnetic moments. Understanding the Heisenberg model beyond ordinary ferromagnetic/antiferromagnetic exchange is of central scientific relevance as higher order interactions are at the core of most of the exotic physical phenomena that could be harnessed in future spintronics devices [6–9]. As an example, the Dzyaloshinskii-Moriya interaction (DMI) [10,11] is known to stabilize skyrmionic/antiskyrmionic structures [12,13] which hold promise as information carriers in novel spintronic memory devices. At the same time, micromagnetic solvers [14] that can then be employed to simulate the magnetization dynamics on the micro-scale rely on continuum formulations making the generalization of the Heisenberg model and its higher order extensions to the continuum [15] of central importance. On the microscopic scale the inclusion of higher order interactions in the Heisenberg model can be done by considering the low energy limit of increasingly complicated multi-band Hubbard models [5]. On a micromagnetic level, the traditional approach relies on phenomenological thermodynamic arguments and spin wave expansions of the micromagnetic energy functional [16–18], but disregards the underlying Heisenberg model in favor of a pure field

theoretical approach. The generalized expression of the micromagnetic energy functional that one finds in the literature is [5,19,20]

$$E_{ex}[\mathbf{m}, \nabla \mathbf{m}] = \int_{\Omega_V} \{A |\nabla \mathbf{m}|^2 + \hat{\mathbf{Q}} \mathcal{M}(\mathbf{m})\} d^3 \mathbf{r}, \quad (1)$$

where $\hat{\mathbf{Q}} \mathcal{M}(\mathbf{m}) = \sum_{A,C} \hat{\mathbf{Q}}_{AC} \mathcal{M}_{AC}$ constitutes the DMI energy of the system [21] and is represented as the contraction of the DMI tensor $\hat{\mathbf{Q}}_{AC}$ and the chirality $\mathcal{M}(\mathbf{m}) = \nabla \mathbf{m} \times \mathbf{m}$ of the material. The above-mentioned approaches, while extremely powerful, are phenomenological in nature and neglect the fact that higher order interactions are intimately related to lower order ones as they come from the low energy limit of a more general energy functional [10]. A formulation of the continuum limit that rigorously and organically keeps track of the coordination of the magnetic atoms on the lattice and higher order interactions is still missing. In this work we propose an alternative procedure to the continuum limit of the Heisenberg model [22] that employs graph theory to systematically account for lattices of arbitrary point group symmetry and local $SO(3)$ gauge invariance of the micromagnetic energy functional to account for the appearance of higher order interactions [23–25]. The outcome is a continuum limit that naturally represents the exchange interaction energy in the most general form at all orders, both in the bulk

^(a)E-mail: g.durin@inrim.it (corresponding author)

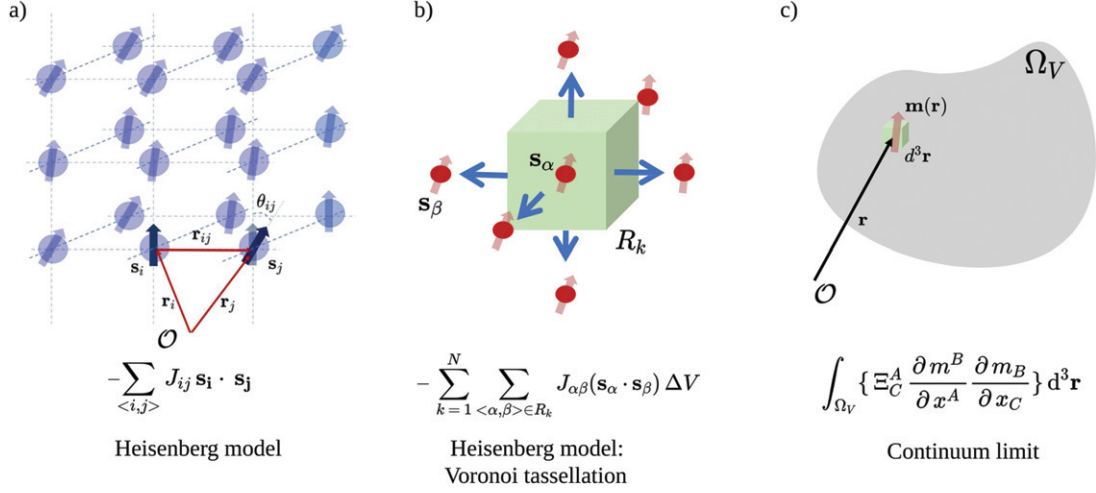


Fig. 1: (a) Heisenberg model on a cubic lattice. We indicate the lattice sites with indices i, j . (b) Decomposition of the cubic lattice in nearest neighbour clusters using the Voronoi tassellation [27]. In this decomposed lattice we use the k index to identify the cell and α, β indices to indicate the nearest neighbours. (c) Continuum limit performed on the cell from (b). The cell index k becomes continuous $d^3\mathbf{r}$ and the atomic moments become a continuous function of space $\mathbf{m}(\mathbf{r})$.

and in thin film geometries,

$$E_{ex} = \int_{\Omega_V} \{ \Xi_{AC} \partial^A m^B \partial^C m_B - Q_{Al} \mathcal{M}^{LA} \} d^3\mathbf{r}, \quad (2)$$

where Ξ_{AC} is the anisotropic symmetric exchange tensor and Q_{Al} is the DMI tensor. The structure of the paper is as follows: in the next section, we reformulate the continuum limit of exchange using graph theory and we rewrite exchange in a form that keeps track of the lattice beyond the simple cubic case. In the third section we require local $SO(3)$ gauge invariance to account for the appearance of the DMI tensor [26]. The Neumann principle of crystallography allows us to derive the non-vanishing components of the anisotropic exchange and micromagnetic DMI for all 32 crystallographic point groups. In the last section we discuss our result and validate our predictions by comparing them with the existing literature and several experimental systems. In the appendix we review the Taylor expansion on discrete lattices and some key concepts of graph theory.

Continuum limit of Heisenberg exchange on arbitrary lattices. – We start by writing the Heisenberg exchange interaction in the usual way,

$$\mathcal{H} = - \sum_{\langle i,j \rangle} J_{ij} \mathbf{s}_i \cdot \mathbf{s}_j, \quad (3)$$

here $J(\mathbf{r}_{ij}) = J_{ij}$ are the coupling coefficients coming from the exchange integral, a function of the distance \mathbf{r}_{ij} from atom i to atom j , see fig. 1(a). We can split the energy sum in the contribution coming from each individual Wigner-Seitz (WS) cell of the lattice labelled R_k (see fig. 1(b)). The advantages of this decomposition are twofold: firstly, the WS cell construction is based in the Voronoi tassellation [27], *i.e.*, on the location of nearest neighbours. Secondly, the WS cell (a primitive cell) for a given lattice

point inherits the full point group symmetry of the lattice by constructions [28],

$$\mathcal{H} = - \sum_{k=1}^N \sum_{\langle \alpha, \beta \rangle \in R_k} J_{\alpha\beta} \mathbf{s}_\alpha \cdot \mathbf{s}_\beta \Delta V, \quad (4)$$

here R_k represents the set of nearest neighbors used for the construction of the k -th WS cell [28,29]. We define \mathcal{E}_k as the energy density cost due to spin misalignment per WS cell with volume ΔV ,

$$\mathcal{E}_k = - \sum_{\langle \alpha, \beta \rangle \in R_k} J_{\alpha\beta} \mathbf{s}_\alpha \cdot \mathbf{s}_\beta, \quad (5)$$

we assume that \mathbf{s}_α and \mathbf{s}_β are nearly parallel when nearest neighbours and have fixed length $|\mathbf{s}|^2 = 1$ (see fig. 1(b)). This allows us to write the exchange term as

$$\mathcal{E}_k = - \sum_{\langle \alpha, \beta \rangle \in R_k} J_{\alpha\beta} |\mathbf{s}|^2 \cos \theta_{\alpha\beta}, \quad \theta_{\alpha\beta} \ll 1 \quad (6)$$

$$\approx - \sum_{\langle \alpha, \beta \rangle \in R_k} J_{\alpha\beta} \delta^{\alpha\beta} - J_{\alpha\beta} |\mathbf{s}_\alpha - \mathbf{s}_\beta|^2. \quad (7)$$

Since we are treating the ferromagnetic case (*i.e.*, $J_{\alpha\beta}$ symmetric positive semi-definite) we can rewrite the exchange matrix as $J_{\alpha\beta} = G_{\alpha n} G_{n\beta} = \hat{G}^T \hat{G}$. We neglect the first term of eq. (7) as it is simply a constant and we can rewrite the exchange energy as

$$\mathcal{E}_k = \sum_{\langle \alpha, \beta \rangle \in R_k} G_{\alpha n} G_{n\beta} |\mathbf{s}_\alpha - \mathbf{s}_\beta|^2, \quad (8)$$

since, for small $\theta_{ij} \approx |\mathbf{s}_i - \mathbf{s}_j|$, we assume that \mathbf{s}_i can be fitted to a continuous function, *i.e.*, $\mathbf{s}_i \rightarrow \mathbf{m}(\mathbf{r} - \mathbf{r}_i)$, of position in the lattice and that, to a sufficient approximation (see eq. (A.2) in the appendix),

$$\mathbf{m}(\mathbf{r} + \mathbf{r}_i) \approx \mathbf{m}(\mathbf{r}) + C_{i\alpha} \mathbf{l}^\alpha \cdot \nabla \mathbf{m}(\mathbf{r}), \quad (9)$$

where $C_{i\alpha}$ represents the incidence matrix of the directed graph describing the nearest neighbor cluster of magnetic atoms (see the Supplementary Material [SupplementaryMaterial.pdf](#) (SM) for the case of a simple cubic lattice), $\mathbf{l}^\alpha = l_A^\alpha \hat{e}^A$ represents the edge vectors of the directed graph and $\nabla = \hat{e}^A \frac{\partial}{\partial x^A}$. With this generalized notation we can write the exchange term of eq. (7) as

$$\mathcal{E}(\mathbf{r}) = \sum_{\langle\alpha,\beta\rangle} \left[G_{\alpha n} C_\gamma^\alpha l_A^\gamma \frac{\partial m^B}{\partial x^A} \right] \left[G_{n\beta} C_\beta^\rho l_C^\rho \frac{\partial m_B}{\partial x^C} \right]. \quad (10)$$

We remark how by transforming the magnetization in a continuous function of space, we automatically promote the energy per cell to a continuous function of space as well, *i.e.*, $\mathcal{E}_k \rightarrow \mathcal{E}(\mathbf{r})$. This also applies to the volume R_k of eq. (8) which is now promoted to an infinitesimal volume element $d^3\mathbf{r}$. We store all the information related to the symmetry of the lattice and the exchange J_{ij} in the (symmetric) anisotropic exchange tensor Ξ^{AC} ,

$$\Xi_{AC} := \sum_{\langle\alpha,\beta\rangle} G_{\alpha n} C_\gamma^\alpha l_A^\gamma G_{n\beta} C_\beta^\rho l_C^\rho. \quad (11)$$

The total exchange energy is now obtained by integrating $\mathcal{E}(\mathbf{r})$ over the whole volume,

$$E_{ex}[\mathbf{m}, \nabla \mathbf{m}] = \int_{\Omega_V} \Xi_{AC} \frac{\partial m_B}{\partial x^C} \frac{\partial m^B}{\partial x^A} d^3\mathbf{r}. \quad (12)$$

In the case of a cubic lattice all the exchange integrals $J_{ij} = J$ are constant and we have $\Xi_{AC} = -2J\delta_{AC}$. We refer to the SM for the detailed calculation of the simple cubic case and the C_{6v} case.

Gauge covariant derivatives and the DMI tensor. – As discussed in [23,26,30], the appearance of DMI in a continuum theory of magnetic interactions is a direct consequence of promoting the global $SO(3)$ symmetry of the micromagnetic energy functional to a local symmetry. The requirement of invariance with respect to a local rotation of the magnetic moment requires the inclusion of a non-Abelian gauge degree of freedom encoded in the modification of the ordinary differential operator $\partial_i := \frac{\partial}{\partial x^i}$. Formally speaking, let $\mathcal{R}(\mathbf{x})$ be an element of $SO(3)$ acting on 3-component vectors such as the local magnetization according to $\mathbf{m}' = \mathcal{R}(\mathbf{x})\mathbf{m}$. Enforcing invariance of the exchange energy of eq. (12) requires us to redefine the differential operator via the covariant derivative \mathcal{D} and the gauge field \mathcal{A} in the following way [23]:

$$\partial^i m^j \rightarrow \mathcal{D}^i m^j = \partial^i m^j - (\mathcal{A}^i)_k m^l \varepsilon_{kl}^j. \quad (13)$$

\mathcal{A}_k designates the k -th component of the non-Abelian gauge potential that transforms according to the rule

$$\mathcal{A}'_k = \mathcal{R}^T \mathcal{A}_k \mathcal{R} + \mathcal{R}^T \partial_k \mathcal{R}, \quad (14)$$

where the rotation matrices \mathcal{R} can be represented via

$$\mathcal{R}(\mathbf{x}) = \exp(i\phi(\mathbf{x})\hat{n} \cdot \mathbf{J}), \quad (15)$$

where $\phi(\mathbf{x})$ is a space-dependent rotation angle, \hat{n} is a rotation axis and the generators of $SO(3)$ are encoded in a vector \mathbf{J} such that $[J_\rho, J_\sigma] = i\varepsilon_{\rho\sigma\nu} J_\nu$. If we limit ourselves to the pure gauge case [26], we can restrict the gauge transformations to

$$\mathcal{A}'_k = \mathcal{R}^T \partial_k \mathcal{R} \quad (16)$$

and obtain the gauge covariant derivative of the form

$$\mathcal{D}^i m^j = \partial^i m^j - \partial^i \psi^l m^k \varepsilon_{ljk}, \quad (17)$$

where ψ^l quantifies the rotation of a vector around the axis \hat{n}_l . Inserting this definition in eq. (10) yields the following expression for the energy density:

$$\mathcal{E}(\mathbf{r}) = \sum_{\langle\alpha,\beta\rangle} \left[G_{\alpha n} C_\gamma^\alpha l_A^\gamma \mathcal{D}^A m^B \right] \left[G_{n\beta} C_\beta^\rho l_C^\rho \mathcal{D}^C m_B \right], \quad (18)$$

and the following expression for the integrated total energy:

$$\begin{aligned} E_{ex}[\mathbf{m}, \nabla \mathbf{m}] &= \int_{\Omega_V} d^3\mathbf{r} \{ \Xi_{AC} \mathcal{D}^A m^B \mathcal{D}^C m_B \} \quad (19) \\ &= \int_{\Omega_V} d^3\mathbf{r} \{ \Xi_{AC} \partial^A m^B \partial^C m_B \\ &\quad - \Xi_{AC} \partial^C \psi^l \varepsilon_{lkB} \underbrace{[(\partial^A m^B) m^k - m^B (\partial^A m^k)]}_{\mathcal{L}^{ABk}} \\ &\quad + \Xi_{AC} \partial^A \psi^l m^k \varepsilon_{lkB} \partial^C \psi^r m^s \varepsilon_{rsB} \}, \quad (20) \end{aligned}$$

where Ξ_{AC} is defined in eq. (11). We highlight how \mathcal{L}^{ABk} represents the usual Lifshitz invariant terms of DMI. We remark how this treatment of micromagnetic interactions also gives rise to a factor of intrinsic anisotropy $\Xi_{AC} \partial^A \psi^l m^k \varepsilon_{lkB} \partial^C \psi^r m^s \varepsilon_{rsB}$ which represents an anisotropic term [30] normally neglected in the literature. If we concentrate on terms of order $\mathcal{O}(\nabla\psi)$ we can rewrite the exchange in eq. (12) as

$$\begin{aligned} E_{ex} &= \int_{\Omega_V} d^3\mathbf{r} \{ \Xi_{AC} \partial^A m^B \partial^C m_B - \Gamma_{kB}^A \mathcal{L}_A^{Bk} \} \\ &\quad + \mathcal{O}((\nabla\psi)^2), \quad (21) \end{aligned}$$

where we have introduced the compact notation

$$\Gamma_{AB}^k := \Xi_{AC} \partial^C \psi^l \varepsilon_{lkB}. \quad (22)$$

We highlight how symmetric anisotropic exchange is contracted in the prefactors Γ_{AB}^k of the DMI Lifshitz invariant, showing how the two orders of interactions cannot be treated separately in accordance with the original microscopic treatment of Moriya [10]. We can now apply the Neumann principle of crystallography [31] to the Γ_{AB}^k prefactors of the Lifshitz invariants in eq. (22) to reveal their independent components. Let $\mathcal{R}^{(\alpha)}$ be the 3-dimensional representation of the point group symmetry associated with the crystal system we are considering (α represents

Non-centrosymmetric Point Group PG (= without inversion center)		
Polar non-chiral PG	Non-polar Non-chiral PG	Enantiomorphic PG = Chiral PG
$(C_3): \begin{pmatrix} 0 & 0 & Q_{13} \\ 0 & 0 & Q_{23} \\ Q_{31} & Q_{32} & 0 \end{pmatrix}$	$(S_4): \begin{pmatrix} Q_{11} & Q_{12} & 0 \\ Q_{12} & -Q_{11} & 0 \\ 0 & 0 & 0 \end{pmatrix}$	$(C_1): \begin{pmatrix} Q_{11} & Q_{12} & Q_{13} \\ Q_{21} & Q_{22} & Q_{23} \\ Q_{31} & Q_{32} & Q_{33} \end{pmatrix} \quad \left. \begin{matrix} (D_4) \\ (D_2) \end{matrix} \right\} \begin{pmatrix} Q_{11} & 0 & 0 \\ 0 & Q_{11} & 0 \\ 0 & 0 & Q_{33} \end{pmatrix}$
$(C_{2v}): \begin{pmatrix} 0 & Q_{12} & 0 \\ Q_{21} & 0 & 0 \\ 0 & 0 & 0 \end{pmatrix}$	$(D_{2d}): \begin{pmatrix} Q_{11} & 0 & 0 \\ 0 & -Q_{11} & 0 \\ 0 & 0 & 0 \end{pmatrix}$	$(C_2): \begin{pmatrix} Q_{11} & Q_{12} & 0 \\ Q_{21} & Q_{22} & 0 \\ 0 & 0 & Q_{33} \end{pmatrix} \quad \left. \begin{matrix} (C_4) \\ (C_6) \\ (C) \end{matrix} \right\} \begin{pmatrix} Q_{11} & Q_{12} & 0 \\ -Q_{12} & Q_{11} & 0 \\ 0 & 0 & Q_{33} \end{pmatrix}$
$\left. \begin{matrix} (C_{3v}) \\ (C_{4v}) \\ (C_{6v}) \end{matrix} \right\} \begin{pmatrix} 0 & Q_{12} & 0 \\ -Q_{12} & 0 & 0 \\ 0 & 0 & 0 \end{pmatrix}$	$\left. \begin{matrix} (C_{3h}) \\ (D_{3h}) \\ (T_d) \end{matrix} \right\} \begin{pmatrix} 0 & 0 & 0 \\ 0 & 0 & 0 \\ 0 & 0 & 0 \end{pmatrix}$	$(D_2): \begin{pmatrix} Q_{11} & 0 & 0 \\ 0 & Q_{22} & 0 \\ 0 & 0 & Q_{33} \end{pmatrix} \quad \left. \begin{matrix} (O) \\ (D_6) \\ (T) \end{matrix} \right\} \begin{pmatrix} Q_{11} & 0 & 0 \\ 0 & Q_{11} & 0 \\ 0 & 0 & Q_{11} \end{pmatrix}$

Fig. 2: DMI tensor components $(\hat{Q})_{ij} := Q_{ij}$ from eq. (24) as a function of all 21 non-centrosymmetric crystallographic point groups as imposed by the Neumann principle of eq. (23). The 11 centrosymmetric point groups have a vanishing DMI tensor and are not shown. The generators are expressed in the basis used in [31].

the index numbering the generators of the group). The Neumann principle [32] imposes

$$\Gamma_{jk}^i = (\mathcal{R}^{(\alpha)})_{i'}^i (\mathcal{R}^{(\alpha)})_j^{j'} (\mathcal{R}^{(\alpha)})_k^{k'} \Gamma_{j'k'}^{i'}, \quad \forall \alpha. \quad (23)$$

We can now extract the non-vanishing components of the DMI tensor $Q_{Al} := \Xi_{AC} \partial^C \psi_l$ by contracting Γ_{AB}^k with the Levi-Civita tensor ε_l^{Bk} and using standard identity $\varepsilon_{ijk} \varepsilon_{ljk} = 2\delta_{il}$ which yields

$$Q_{Al} = -\frac{1}{2} \Gamma_{AB}^k \varepsilon_{lk}^B. \quad (24)$$

This formula now allows to systematically predict the shape of the DMI tensor for all 32 crystallographic point groups. Using the generators for the crystallographic point groups contained in [33] we arrive at DMI tensors Q_{Al} of the form shown in fig. 2. With this we get the final form of the exchange energy functional of eq. (2),

$$E_{ex} = \int_{\Omega_V} \{ \Xi_{AC} \partial^A m^B \partial^C m_B - Q_{Al} \mathcal{M}^{lA} \} d^3 \mathbf{r} \quad (25)$$

where the chirality is given by $\mathcal{M}^{lA} = \varepsilon_{kB}^l \mathcal{L}^{ABk}$. We remark how the Neumann principle can also be applied to the $\hat{\Xi}$ tensor from eq. (11),

$$\Xi_{ij} = (\mathcal{R}^{(\alpha)})_i^{i'} (\mathcal{R}^{(\alpha)})_j^{j'} \Xi_{i'j'}, \quad (26)$$

revealing the non-vanishing components of symmetric exchange shown in fig. 3.

DMI tensor decomposition and ground state selection criterion. – We now proceed to describe some of the physical consequences of the symmetry properties of the DMI tensor written in the form of eq. (24) [26]. First of all we note that the DMI tensor \hat{Q} , much like any rank-2 tensor, can be decomposed as a sum of symmetric and

skew-symmetric components,

$$\hat{Q} = \underbrace{\frac{1}{2}(\hat{Q} - \hat{Q}^T)}_{\hat{Q}_A} + \underbrace{\frac{1}{2}(\hat{Q}^T + \hat{Q})}_{\hat{Q}_S}. \quad (27)$$

A purely anti-symmetric DMI tensor yields Lifshitz invariant terms of the form

$$\mathcal{E}_{A;DMI} = -2\mathbf{D} \cdot [\mathbf{m}(\nabla \cdot \mathbf{m}) - (\nabla \cdot \mathbf{m})\mathbf{m}], \quad (28)$$

where one expresses the anti-symmetric tensor as $(Q_A)_{ij} = D_k \varepsilon_{kij}$. This term corresponds to the continuum limit of the familiar microscopic interfacial DMI term [12,34],

$$\mathcal{H}_{DMI} = \sum_{(i,j)} \mathbf{D}_{ij} \cdot (\mathbf{s}_i \times \mathbf{s}_j), \quad (29)$$

where \mathbf{s}_i represents a magnetic moment located at lattice site i and \mathbf{D}_{ij} is the DMI contribution to the Heisenberg Hamiltonian. Lifshitz invariant terms of the form eq. (28) correspond to the surface DMI term appearing in magnetic thin films [35]. The symmetric component of the DMI tensor yields an energy contribution of the form

$$\mathcal{E}_{S;DMI} = -\mathbf{m} \cdot (\hat{Q}_S \nabla \times \mathbf{m}), \quad (30)$$

where $\hat{Q}_S \nabla = (Q_S)_{ij} \partial_j$. The special case of a purely diagonal matrix yields an energy term of the form

$$\mathcal{E}_{S;DMI} = -2(Q_S)_{ii} (\mathbf{m} \cdot \partial_i \mathbf{m})_i, \quad (31)$$

which, in the case of a single independent component $Q_{ii} = D \forall i$ yields

$$\mathcal{E}_{S;DMI} = -2D \mathbf{m} \cdot (\nabla \times \mathbf{m}). \quad (32)$$

This energy contribution corresponds to a bulk DMI term responsible for stabilizing bulk chiral structures [13,21,26].

Symmetric exchange components $\hat{\Xi}$		
$\left. \begin{array}{l} C_1 \\ C_i \end{array} \right\} \begin{pmatrix} \Xi_{11} & \Xi_{12} & \Xi_{13} \\ \Xi_{12} & \Xi_{22} & \Xi_{23} \\ \Xi_{13} & \Xi_{23} & \Xi_{33} \end{pmatrix}$	$\left. \begin{array}{l} D_2, C_{2v}, D_{2h}, \\ C_4, S_4, C_{4h}, \\ D_4, C_{4v}, D_{2d}, \\ D_{4h}, C_3, S_6, \\ D_3, C_{3v}, D_{3d}, \\ C_6, C_{3h}, C_{6h}, \\ D_6, C_{6v}, D_{3h}, \\ D_{6h} \end{array} \right\}$	$\left. \begin{array}{l} T, T_h, \\ O, T_d, \\ O_h \end{array} \right\} \begin{pmatrix} \Xi_{11} & 0 & 0 \\ 0 & \Xi_{11} & 0 \\ 0 & 0 & \Xi_{33} \end{pmatrix}$
$\left. \begin{array}{l} C_2 \\ C_s \\ C_{2h} \end{array} \right\} \begin{pmatrix} \Xi_{11} & \Xi_{12} & 0 \\ \Xi_{12} & \Xi_{11} & 0 \\ 0 & 0 & \Xi_{11} \end{pmatrix}$	$\left. \begin{array}{l} D_2, C_{2v}, D_{2h}, \\ C_4, S_4, C_{4h}, \\ D_4, C_{4v}, D_{2d}, \\ D_{4h}, C_3, S_6, \\ D_3, C_{3v}, D_{3d}, \\ C_6, C_{3h}, C_{6h}, \\ D_6, C_{6v}, D_{3h}, \\ D_{6h} \end{array} \right\}$	$\left. \begin{array}{l} T, T_h, \\ O, T_d, \\ O_h \end{array} \right\} \begin{pmatrix} \Xi_{11} & 0 & 0 \\ 0 & \Xi_{11} & 0 \\ 0 & 0 & \Xi_{11} \end{pmatrix}$

Fig. 3: Symmetric exchange components $\hat{\Xi}_{ij} := \Xi_{ij}$ from eq. (11) as a function of all 32 crystallographic point groups as imposed by the Neumann principle (23). The generators are expressed in the basis used in [31].

As discussed in [21], the shape of the DMI tensor is a decisive factor in determining the appearance of skyrmionic or antiskyrmionic structures in the ground state of magnetic materials. The main result of [21] is the identification of the determinant of the DMI tensor as the relevant quantity predicting the stability of skyrmions or anti-skyrmions as follows:

$$\det(\hat{Q}) \begin{cases} < 0, & \text{anti-skyrmions stabilized,} \\ > 0, & \text{skyrmions stabilized,} \\ = 0, & \text{coexistence.} \end{cases} \quad (33)$$

We can now apply this rule to the set of DMI tensors shown in fig. 2 and discuss if the predicted ground state structures are compatible with experimental results discussed in the literature.

Discussion. – The structure of eq. (24) automatically implies that all centrosymmetric crystallographic point groups exclude the possibility to have DMI. Furthermore, we notice how the above-discussed method also correctly predicts the absence of DMI on some non-centrosymmetric crystal systems such as T_d, C_{3h}, D_{3h} in accordance with the literature [19]. We can now proceed and discuss three examples of a non-vanishing DMI tensor. MnSi is a magnetic material which has attracted a lot of attention as it is one of the first materials in which the presence of helical magnetic order was detected. As known from the literature, at low temperatures MnSi can be modelled using the extended classical Heisenberg model [36] and the system is known to crystallize in a B20 structure [37]. If we isolate the magnetic atoms of this material, *i.e.*, the Mn atoms, the resulting sublattice displays T point group symmetry [38]. From fig. 2, we can see how the T point group symmetry allows the material to have a purely diagonal DMI tensor which can be linked to the presence of bulk DMI, a form compatible with the appearance of bulk

chiral magnetism [13,26,37],

$$\hat{Q}_T = \begin{pmatrix} Q_{11} & 0 & 0 \\ 0 & Q_{11} & 0 \\ 0 & 0 & Q_{11} \end{pmatrix} \quad (34)$$

$$\Rightarrow \mathcal{E}_{S;DMI} = -2Q_{11} \mathbf{m} \cdot (\nabla \times \mathbf{m}). \quad (35)$$

If we want to consider only thin film geometries in which the growth direction lies parallel to the \hat{z} -axis, we simply have to consider the top left submatrix,

$$\hat{Q}_T[1, 2; 1, 2] = \begin{pmatrix} Q_{11} & 0 \\ 0 & Q_{11} \end{pmatrix}, \quad (36)$$

and the determinant of this submatrix is strictly positive. Recalling the selection criterion of eq. (33) [21], we know that a strictly positive determinant of the DMI tensor stabilizes skyrmions given the presence of a sufficiently high external field [38]. Further examples of applicability of the present formalism concern Heusler alloys [39–41]. Despite the full Heusler structure displaying cubic symmetry (and therefore no DMI), recent studies have shown how altering the Mn concentration in inverse tetragonal Mn-based Heusler compounds such as Mn_xPtSn can lower the symmetry of the material as much as reaching D_{2d} [42] in thin film geometries. The DMI tensor of the D_{2d} symmetry group from fig. 2 has a symmetric traceless form

$$\hat{Q}_{D_{2d}} = \begin{pmatrix} Q_{11} & 0 & 0 \\ 0 & -Q_{11} & 0 \\ 0 & 0 & 0 \end{pmatrix}. \quad (37)$$

Much like in the case of MnSi, restricting the DMI tensor to a thin film geometry in which the growth direction lies parallel to the \hat{z} -axis yields

$$\hat{Q}_{D_{2d}}[1, 2; 1, 2] = \begin{pmatrix} Q_{11} & 0 \\ 0 & -Q_{11} \end{pmatrix}. \quad (38)$$

We immediately notice how $\det(\hat{Q}_{D_{2d}}[1, 2; 1, 2]) = -Q_{11}^2 < 0$. Again, according to eq. (33) this DMI tensor can only stabilize antiskyrmions (given a sufficiently

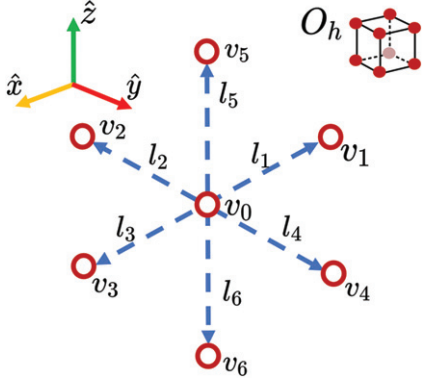


Fig. 4: Directed graph representing the nearest neighbors (n.n.) on the cubic lattice. The vertices are represented by v_i and the edges by l_i .

high external field). It has in fact been experimentally shown that Mn_xPtSn thin films can only support anti-skyrmions structures [40]. As a final case of interest, we consider heavy metal/ferromagnet (HM/FM) multilayers such as Pt(111)/Co which have been under intense scientific investigation for the development of energy efficient magnetic memory storage devices [43,44]. In such systems, one of the effects of the inclusion/exclusion of the Pt layer is that of reducing the point group symmetry of the Co layer from D_{6h} to C_{3v} which, in terms of DMI tensors from fig. 2, means

$$\hat{Q}_{D_{6h}} = \begin{pmatrix} 0 & 0 & 0 \\ 0 & 0 & 0 \\ 0 & 0 & 0 \end{pmatrix} \rightarrow \hat{Q}_{C_{3v}} = \begin{pmatrix} 0 & Q_{12} & 0 \\ -Q_{12} & 0 & 0 \\ 0 & 0 & 0 \end{pmatrix}. \quad (39)$$

This immediately highlights how the broken inversion symmetry can cause the emergence of DMI interaction at Pt/Co(111) interfaces. At the same time, we notice how $\det(\hat{Q}_{C_{3v}}) > 0$ and therefore only skyrmions can be stabilized [43,45]. As an aside, we also remark how the applications of strain gradients [46] and electric fields [24] to materials displaying chiral interactions can alter the properties of the DMI tensor. In particular, strong electric fields can lead to the change of the antisymmetric components of the DMI tensor [23] and could therefore constitute a way to manipulate skyrmions and antiskyrmions in an energy efficient way.

Conclusions. – In this work we presented a new perspective on the continuum limit of the classical Heisenberg model to derive the micromagnetic exchange energy functional. Our approach systematically keeps track of the crystal symmetries of the system and reveals the importance of the interplay between symmetric anisotropic exchange and DMI. We show a rigorous treatment of higher order interactions when promoting the symmetry of the Hamiltonian from global to local via the introduction of gauge covariant derivatives [23,26]. As an example, we show how the symmetry constraints imposed by the lattice

can be implemented rigorously via the Neumann principle of crystallography, revealing the independent components of the DMI tensor for all 32 crystallographic point groups. We point out how the determinant of the DMI tensor can be used as a tool to predict the stabilization of skyrmions and antiskyrmions [21] and we observe how several experimental results behave in accordance with our theoretical predictions.

Data availability statement: No new data were created or analysed in this study.

Appendix: Taylor expansion with discrete calculus using graph theory. – In the following we review the Taylor expansion of discrete calculus [47] in order to motivate our derivation of the continuum limit of micromagnetic exchange in the next section. In the following we are going to employ the Einstein summation convention for repeating indices. Let us write down the general expression for the Taylor expansion of the magnetization vector field for small $\Delta\mathbf{r}$,

$$\mathbf{m}(\mathbf{r} + \Delta\mathbf{r}) \approx \mathbf{m}(\mathbf{r}) + d\mathbf{m}(\mathbf{r}; \Delta\mathbf{r}) + \mathcal{O}(|\Delta\mathbf{r}|^2) \quad (\text{A.1})$$

where $d\mathbf{m}(\mathbf{r}; \Delta\mathbf{r})$ represents the directional derivative of the vector valued function $\mathbf{m}(\mathbf{r})$ along the vector $\Delta\mathbf{r}$, *i.e.*,

$$dm_i(\mathbf{r}; \Delta\mathbf{r}) = \nabla m_i \cdot \Delta\mathbf{r} = \partial_j m_i \Delta r_j. \quad (\text{A.2})$$

We now formally define a nearest-neighbour cluster of atoms as a directed graph (see fig. 4 for an example of the cubic lattice) introducing the edge-node incidence matrix C_{ij} [47] defined as

$$C_{ij} = \begin{cases} 0, & \text{if edge } i \text{ and node } j \text{ are not connected,} \\ +1, & \text{if edge } i \text{ is directed toward node } j: i \rightarrow j, \\ -1, & \text{if edge } i \text{ is directed out of node } j: i \leftarrow j. \end{cases}$$

It can be shown [47] that the incidence matrix of a graph is the natural matrix representation of the discrete differential. Let us now denote the edges of the directed graph representing the lattice as \mathbf{l}^i (see fig. 4), we can generalize eq. (A.2) to

$$d\mathbf{m}(\mathbf{r}; \Delta\mathbf{r}) = (\nabla_k m_i) C_{kj} \mathbf{l}^j \quad (\text{A.3})$$

and finally write the components of the expansion (A.1) as

$$m_i(\mathbf{r} + \Delta\mathbf{r}) \approx m_i(\mathbf{r}) + (\nabla_k m_i(\mathbf{r})) C_{kj} \mathbf{l}^j + \mathcal{O}(\nabla \mathbf{m}). \quad (\text{A.4})$$

REFERENCES

- [1] STANLEY H. E., *Phys. Rev. Lett.*, **20** (1968) 589.
- [2] NOWAK U., *Classical spin models*, in *Handbook of Magnetism and Advanced Magnetic Materials*, edited by KRONMÜLLER H., PARKIN S., MILTAT J. and SCHEINFELD M. (John Wiley & Sons, Ltd.) 2007.

- [3] WYSIN G. M., *Magnetism theory: Spin models*, in *Magnetic Excitations and Geometric Confinement* (IOP Publishing) 2015, pp. 1–47.
- [4] CLEVELAND C. L. and MEDINA A. R., *Am. J. Phys.*, **44** (1976) 44.
- [5] HOFFMANN M. and BLÜGEL S., *Phys. Rev. B*, **101** (2020) 024418.
- [6] VEDMEDENKO E. Y., KAWAKAMI R. K., SHEKA D. D., GAMBARDELLA P., KIRILYUK A., HIROHATA A., BINEK C., CHUBYKALO-FESENKO O., SANVITO S., KIRBY B. J., GROLLIER J., EVERSCHOR-SITTE K., KAMPFRATH T., YOU C. Y. and BERGER A., *J. Phys. D: Appl. Phys.*, **53** (2020) 453001.
- [7] HELLMAN F., DIVISION M. S., BERKELEY L., HOFFMANN A., BEACH G. S. D., FULLERTON E. E., MACDONALD A. H. and RALPH D. C., *Rev. Mod. Phys.*, **89** (2017) 025006.
- [8] LUO S. and YOU L., *APL Mater.*, **9** (2021) 050901.
- [9] WALKER B. W., CUI C., GARCIA-SANCHEZ F., INCORVIA J. A. C., HU X. and FRIEDMAN J. S., *Appl. Phys. Lett.*, **118** (2021) 192404.
- [10] MORIYA T., *Phys. Rev.*, **120** (1960) 91.
- [11] DZYALOSHINSKY I., *J. Phys. Chem. Solids*, **4** (1958) 241.
- [12] FERT A., CROS V. and SAMPAIO J., *Nat. Nanotechnol.*, **8** (2013) 152.
- [13] NAGAOSA N. and TOKURA Y., *Nat. Nanotechnol.*, **8** (2013) 899.
- [14] VANSTEENKISTE A., LELIAERT J., DVORNIK M., HELSEN M., GARCIA-SANCHEZ F. and WAEYENBERGE B. V., *AIP Adv.*, **4** (2014) 107133.
- [15] BROWN W., *Micromagnetics* (J. Wiley, New York, London) 1963.
- [16] BOGDANOV A. N., RÖSSLER U. K., WOLF M. and MÜLLER K.-H., *Phys. Rev. B*, **66** (2002) 214410.
- [17] BAK P. and JENSEN M. H., *J. Phys. C: Solid State Phys.*, **13** (1980) L881.
- [18] LANDAU L. D. and LIFSHITZ E., *Statistical Physics* (Elsevier, Amsterdam) 1980.
- [19] ULLAH A., BALAMURUGAN B., ZHANG W., VALLOPILLY S., LI X.-Z., PAHARI R., YUE L.-P., SOKOLOV A., SELLMYER D. J. and SKOMSKI R., *IEEE Trans. Magn.*, **55** (2019) 7100305.
- [20] LEONOV A. O., MONCHESKY T. L., ROMMING N., KUBETZKA A., BOGDANOV A. N. and WIESENDANGER R., *New J. Phys.*, **18** (2016) 065003.
- [21] HOFFMANN M., ZIMMERMANN B., MÜLLER G. P., SCHÜRHOFF D., KISELEV N. S., MELCHER C. and BLÜGEL S., *Nat. Commun.*, **8** (2017) 308.
- [22] KRONMÜLLER H., *General Micromagnetic Theory and Applications*, in *Materials Science and Technology* (Wiley, London) 2019, pp. 1–43.
- [23] ANSALONE P., PERNA S., D'AQUINO M., SCALERA V., SERPICO C. and BASSO V., *IEEE Trans. Magn.*, **58** (2022) 7100404.
- [24] BASSO V. and ANSALONE P., *EPL*, **130** (2020) 17008.
- [25] GUSLIENKO K. Y., *EPL*, **113** (2016) 67002.
- [26] ANSALONE P., OLIVETTI E. S., MAGNI A., SOLA A. and BASSO V., *EPL*, **3** (2022) 035135.
- [27] GOODMAN J. E., O'ROURKE J. and TÓTH C. D., *Handbook of Discrete and Computational Geometry*, third edition (Chapman and Hall/CRC, New York) 2017.
- [28] ASHCROFT N. W. and MERMIN N. D., *Solid State Physics* (Holt-Saunders, Philadelphia) 1976.
- [29] WIGNER E. and SEITZ F., *Phys. Rev.*, **43** (1933) 804.
- [30] HILL D., SLASTIKOV V. and TCHERNYSHYOV O., *SciPost Phys.*, **10** (2021) 078.
- [31] BIRSS R. R., *Symmetry and Magnetism* (North-Holland Pub, Amsterdam) 1966.
- [32] BHAGAVANTAM S. and PANTULU P. V., *Proc. Indian Acad. Sci. Sect. A*, **66** (1967) 33.
- [33] AROYO M. I., PEREZ-MATO J. M., CAPILLAS C., KROUMOVA E., IVANTCHEV S., MADARIAGA G., KIROV A. and WONDRATSCHEK H., *Z. Kristallogr. Cryst. Mater.*, **221** (2006) 15.
- [34] YANG H., THIAVILLE A., ROHART S., FERT A. and CHSHIEV M., *Phys. Rev. Lett.*, **115** (2015) 267210.
- [35] THIAVILLE A., ROHART S., JUÉ É., CROS V. and FERT A., *EPL*, **100** (2012) 57002.
- [36] HALL K. P. and CURNOE S. H., *Phys. Rev. B*, **104** (2021) 1.
- [37] ISHIKAWA Y., TAJIMA K., BLOCH D. and ROTH M., *Solid State Commun.*, **19** (1976) 525.
- [38] RÖSSLER U. K., BOGDANOV A. N. and PFLEIDERER C., *Nature*, **442** (2006) 797.
- [39] GALANAKIS I., *Theory of Heusler and full-Heusler compounds*, in *Heusler Alloys*, edited by FELSNER C. and HIROHATA A., *Springer Series in Materials Science*, Vol. **222** (Springer, Cham) 2015, pp. 3–36.
- [40] SINGH D. and VERMA K. C., *Magnetic properties of Heusler alloys and nanoferrites*, in *Magnetic Skyrmions*, edited by SAHU D. R. (IntechOpen, Rijeka) 2021, Chapt. 5.
- [41] ELPHICK K., FROST W., SAMIEPOUR M., KUBOTA T., TAKANASHI K., SUKEGAWA H., MITANI S. and HIROHATA A., *Sci. Technol. Adv. Mater.*, **22** (2021) 235.
- [42] SWEKIS P., GAYLES J., KRIEGNER D., FECHER G. H., SUN Y., GOENNENWEIN S. T., FELSNER C. and MARKOU A., *ACS Appl. Electron. Mater.*, **3** (2021) 1323.
- [43] YANG H., THIAVILLE A., ROHART S., FERT A. and CHSHIEV M., *Phys. Rev. Lett.*, **115** (2015) 267210.
- [44] DEGER C., *Sci. Rep.*, **10** (2020) 1.
- [45] WANG L., LIU C., MEHMOOD N., HAN G., WANG Y., XU X., FENG C., HOU Z., PENG Y., GAO X. *et al.*, *ACS Appl. Mater. Interfaces*, **11** (2019) 12098.
- [46] KITCHAEV D. A., BEYERLEIN I. J. and VAN DER VEN A., *Phys. Rev. B*, **98** (2018) 3.
- [47] GRADY L. J. and POLIMENI J. R., *Discrete Calculus* (Springer London, London) 2010.